



Photoluminescence-Based Bioassay With Cysteamine-Capped TiO₂ Nanoparticles for the Selective Recognition of *N*-Acyl Homoserine Lactones

Sahana Vasudevan¹, Parthasarathy Srinivasan^{2,3}, Prasanna Neelakantan⁴, John Bosco Balaguru Rayappan^{2*} and Adline Princy Solomon^{1*}

¹Quorum Sensing Laboratory, Centre for Research in Infectious Diseases (CRID), School of Chemical and Biotechnology, SASTRA Deemed to be University, Thanjavur, India, ²Nanosensors Laboratory, School of Electrical & Electronics Engineering, Centre for Nanotechnology & Advanced Biomaterials (CeNTAB), SASTRA Deemed University, Thanjavur, India, ³Department of Electronics and Communication Engineering, Amrita School of Engineering, AMRITA Vishwa Vidyapeetham Chennai Campus, Chennai, India, ⁴Faculty of Dentistry, The University of Hong Kong, Pokfulam, Hong Kong SAR, China

OPEN ACCESS

Edited by:

Tuhin Subhra Santra,
Indian Institute of Technology Madras,
India

Reviewed by:

Tohid Mahmoudi,
Tabriz University of Medical
Sciences, Iran
Kang Mao,
Institute of Geochemistry (CAS), China

*Correspondence:

John Bosco Balaguru Rayappan
rjbosco@ece.sastra.edu
Adline Princy Solomon
adlineprinzy@sastra.ac.in

Specialty section:

This article was submitted to
Biosensors and Biomolecular
Electronics,
a section of the journal
Frontiers in Bioengineering and
Biotechnology

Received: 31 July 2021

Accepted: 08 November 2021

Published: 03 December 2021

Citation:

Vasudevan S, Srinivasan P,
Neelakantan P, Rayappan JBB and
Solomon AP (2021)
Photoluminescence-Based Bioassay
With Cysteamine-Capped TiO₂
Nanoparticles for the Selective
Recognition of *N*-Acyl
Homoserine Lactones.
Front. Bioeng. Biotechnol. 9:750933.
doi: 10.3389/fbioe.2021.750933

Currently available diagnostic procedures for infections are laborious and time-consuming, resulting in a substantial financial burden by increasing morbidity, increased costs of hospitalization, and mortality. Therefore, innovative approaches to design diagnostic biomarkers are imperative to assist in the rapid and sensitive diagnosis of microbial infections. Acyl homoserine lactones (AHLs) are ubiquitous bacterial signaling molecules that are found to be significantly upregulated in infected sites. In this pioneering work, we have developed a simple photoluminescence-based assay using cysteamine-capped titanium oxide (TiO₂) nanoparticles for AHL detection. The PL intensity variation of the oxygen defect state of TiO₂ was used for the biosensing measurements. The bioassays were validated using two well-studied AHL molecules (C4-HSL and 3-oxo-C12 HSL) of an important human pathogen, *Pseudomonas aeruginosa*. The developed system has a maximum relative response of 98%. Furthermore, the efficacy of the system in simulated host urine using an artificial urine medium showed a linear detection range of 10–160 nM. Also, we confirmed the relative response and specificity of the system in detecting AHLs produced by *P. aeruginosa* in a temporal manner.

Keywords: TiO₂ nanoparticles, quorum sensing, acyl homoserine lactone, *Pseudomonas aeruginosa*, photoluminescence

1 INTRODUCTION

Quorum sensing (QS) is a well-synchronized communication process that exists among bacteria to mediate the infection process in the host niches (Azimi et al., 2020). Such communications are established either through the chemical (*N*-acyl homoserine lactones; AHLs) or peptide (auto-inducing peptides; AIPs) cues by the Gram-negative and Gram-positive bacteria, respectively (Rutherford and Bassler, 2012). The quorum of bacterial pathogens directly correlates with the signal concentration, reaching a threshold to attract more and more respondents of its own (intra-species) or from other species (inter-species) with its specific receptor. More specifically, this group

behavior often pertains to the upregulation of virulence genes altering the host niches towards a favorable environment for its survival.

It is well known that AHLs are the key players for Gram-negative bacterial communication. AHLs structurally consist of a lactone ring with varying lengths of carbon tail that are species-specific. The selectivity and specificity among the different AHLs produced by the respective Gram-negative organisms in the polymicrobial environment are based on the carbon length variation (Papenfort and Bassler, 2016). A classic example of AHL-based communication is *Pseudomonas aeruginosa*, which is the predominant infectious agent of cystic fibrosis (Lee and Zhang, 2015) and is also a dominant pathogen found in chronic wound infections (Klockgether and Tümmler, 2017), urinary tract infections (Mittal et al., 2009), and bacteremia (Tuon et al., 2012). This bacterium produces two AHL signals, C4-HSL and 3-oxo-C12 HSL. C4-HSL is synthesized by the AHL synthase enzyme, RhII, and identified by the cognate receptor, RhIR. Similarly, 3-oxo-C12 HSL is synthesized and determined by LasI and LasR, respectively (Papenfort and Bassler, 2016).

Despite the close associations between these signaling systems, the receptors are specific only to their respective signaling molecules (Schuster et al., 2003). This has multiple advantages in terms of the genetic economy and monitoring the bacterial population. In addition to the activation of its virulence mechanism, AHL molecules can activate the gene expression of bacteria, which cannot produce signaling molecules (Subramoni and Venturi, 2009). Thus, AHL molecules help in maintaining the symbiotic relationship among different species. The presence of such AHL molecules is often found in clinical samples such as cystic fibrosis sputum (Azimi et al., 2020) and oral cavity (Muras et al., 2020). This forms a solid basis for our hypothesis that AHL molecules can be exploited as biomarkers for diagnosing an infectious environment. Since AHL molecules are extracellular products, with proper detection systems, they can be detected in a non-invasive manner. Previous studies on AHL detection were dependent on the bacterial biosensor methods (Kawaguchi et al., 2008; Struss et al., 2010; Wu et al., 2021) and the use of physicochemical techniques, which are time-consuming and require high-end instruments for detection (Kumari et al., 2008; Mukherji et al., 2013; Chahande et al., 2021). In addition, bacterial-based biosensors require periodical activation for a stable response (Steindler and Venturi, 2007). Recently, the use of nanomaterials for AHL detection was explored in different platforms. To detect food-borne pathogens, Sun and his coworkers studied the use of quantum dots and its inherent luminescence properties to detect AHL with improved selectivity and limits of detection, tested in the bacterial growth media conditions (Habimana et al., 2018; Yang et al., 2020). Furthermore, the same group explored electrochemical AHL biosensors using metal oxide nanostructures, specifically iron oxide nanomaterials combined with molecular imprinting technology (Jiang et al., 2016). These studies have opened the possibility of integrating nanotechnology-based optical biosensing in AHL detection.

In this context, the current study explores metal oxide nanostructures for AHL detection. Metal oxide nanostructures offer an excellent biosensing platform, owing to optical

properties, ease of functionalization and morphological modifications (Solanki et al., 2011; Jo and Shin, 2020). Among the metal oxides, ZnO and TiO₂ nanoparticles are very well exploited for optical biosensing applications, mainly photoluminescence-based biosensing. Our previous report on functionalized ZnO nanoparticles for AHL sensing proved that metal oxide nanostructured interfaces are the perfect choice for AHL sensing (Vasudevan et al., 2020). It was proved that oxygen vacancies are a vital factor for the AHL detection, which is substantial in TiO₂ having a wide bandgap (3.0–3.2 eV) (Haider et al., 2019; Kang et al., 2019). Additionally, the isoelectric point of TiO₂ (5.8) (McNamee et al., 2005) is much lower than that of ZnO (10.3) (Marsalek, 2014), which might play a decisive role in the interaction with cysteamine (Ma et al., 2020) and, thus, sensitivity. Considering these two parameters, the current work investigates the TiO₂ metal oxide matrix with cysteamine for AHL sensing. TiO₂ is most opted for its optical transmittance and chemical stability in harsh environments. Previous studies have reported the use of TiO₂ nanostructures for PL-based detection of leucosis (Viter et al., 2012), BSA and DNA (Ensafi et al., 2015). TiO₂ is much explored for the development of PL-based immunosensor to detect rabbit IgG and antigen of *Salmonella* sp. (Viter et al., 2017). In this context, the present study focuses on capping of TiO₂ nanoparticles with an FDA-approved linker molecule, cysteamine, to detect AHL molecules. In addition to its role in critical physiological processes (Wan et al., 2011), this simple aminothiol has been used as a linker molecule due to its reactive groups (Sharon, 2014; Tayebi et al., 2016; Tavakkoli Yarakhi et al., 2017; Oliva et al., 2018). In particular, there are reports that have augmented cysteamine as a linker molecule between TiO₂ and gold nanoparticles to enhance the adsorption of gold nanoparticles onto the TiO₂ surface (Park, 2011).

With this as the rationale, the present study aims to cap TiO₂ nanoparticles with cysteamine for the effective detection of AHL molecules. Two variants of the AHL molecule, C4-HSL (short) and 3-oxo-C12 HSL (long), which are typically synthesized by *P. aeruginosa*, are chosen for the present study. The biosensing system established its selective and specific nature in the presence of artificial urine media (AUM) and the presence of *P. aeruginosa*. This interdisciplinary work combines the aspects of nanotechnology and microbiology to provide a fast and accurate diagnostic platform for the infectious environment. The advantages such as non-invasive sample collection, no sample processing and immediate results, overcome the shortcomings of the conventional microbiological techniques. Through this study, for the first time, we have demonstrated the real-time sensing of AHL through PL studies with cysteamine-capped TiO₂ nanoparticles bioassay.

2 MATERIALS AND METHODS

2.1 Synthesis and Functionalization of TiO₂ Nanoparticles

Nanocrystalline TiO₂ was synthesized using the hydrothermal method by employing titanium (IV) isopropoxide and sodium

hydroxide (NaOH) as starting materials (Venkataprasad et al., 2020). Titanium (IV) isopropoxide (1 M) was added to 25 ml of distilled water, and subsequently, 2 M NaOH was added dropwise. This solution was kept under constant stirring for 30 min. The final volume was adjusted to 40 ml using distilled water. The hydrothermal reaction was carried out by heating of the solution up to 240°C for 12 h. Then, the final precipitate was washed several times with distilled water and dried at 450°C for 3 h to obtain nanocrystalline TiO₂ nanoparticles.

The functionalization/capping was carried out by suspending the TiO₂ nanoparticles and the linker molecule, cysteamine, in ethanol. Three different molar ratios of TiO₂-Cysteamine (TiO₂-Cys) were considered—1:0.5, 1:1, and 0.5:1—and sonicated for 12 h to obtain a homogenous cysteamine functionalized nanoparticle solution as reported in our previous study (Vasudevan et al., 2020).

2.2 Material Characterization

The structural analysis of the synthesized and functionalized nanoparticles was studied using an x-ray diffractometer (XRD, D8 Focus, Bruker, Germany). Oxidation states and atomic compositions of the synthesized and functionalized nanoparticles were examined using an x-ray photoelectron spectrometer (Thermo Fisher Scientific Inc., K Alpha, USA). Morphological studies of the synthesized and functionalized nanoparticles were characterized using a field emission transmission electron microscope (FE-TEM, JEM 2100 F, JEOL, Japan). The surface defects of the TiO₂ nanoparticles and functionalized nanoparticles were investigated using a PL spectrophotometer (FP-8200, JASCO, USA). Functional group analysis of the prepared and functionalized nanoparticle was studied using the Fourier transform infrared spectrometer (FT-IR, Alpha-T, Bruker, Germany).

2.3 Bio-Analyte, Bacterial Culture, and Media Preparation

C4-HSL (N-Butyryl-DL-homoserine lactone, ≥96.0%) and 3-Oxo-C12-HSL [N-(3-oxododecanoyl)-homoserine lactone, ≥96.0%] were obtained from Sigma Aldrich, USA. The stock solutions of 1 M were prepared in dimethyl sulfoxide (DMSO, Sigma Aldrich).

The bacterial strain *P. aeruginosa* (MCC 3101) was maintained as a glycerol stock at -80°C. The AUM was prepared by adding the components (Supplementary Table S1) in the sterile distilled water and filter sterilized (Brooks and Keevil, 1997). The pH of the media was adjusted using 1 M NaOH (HiMedia Laboratories, USA) and concentrated hydrochloric acid solution (SRL, India).

2.4 Photoluminescence Biosensing Measurements

The detailed description of the biosensing measurements were carried out as described previously (Vasudevan et al., 2020) using PL spectrophotometer (FP-8200, JASCO, USA). The following are the PL parameters used by maintaining the emission and excitation bandwidth of 5 nm throughout. TiO₂ nanoparticles

were excited at the wavelength of 320 nm, and the emission spectra were observed in the range of 350–550 nm. Other conditions like the detector's response time of 1 s and recording speed of 500 nm min⁻¹ were maintained throughout. The PL spectra of TiO₂ nanoparticles, TiO₂-Cys, and TiO₂-Cys in the presence of two AHLs (C4 and 3-oxo-C12) were recorded to determine the response. The relative response of the biosensor was calculated as below:

$$RR = \frac{R_A - R_B}{R_A} \times 100\% \quad (1)$$

Where *RR* denotes the relative response, *R_A* is the peak intensity of TiO₂-Cys in the presence of AHL, and *R_B* denotes the peak intensity of TiO₂-Cys in the absence of AHL. The AHL concentrations were varied from 10 to 40 nM to establish the linear response between the relative response and AHL concentration. For the host simulated environment, AUM, the same protocol was used. AHL concentrations from 10 nM–1 μM were dispersed in AUM and validated for the specificity and relative response.

2.5 Real-Time Analysis of TiO₂-Cys With *P. aeruginosa*

TiO₂-Cys was tested to identify the HSL synthesized by the clinical isolate of (human kidney stone) *P. aeruginosa*, MCC3101. The initial inoculum of the *P. aeruginosa* was prepared in AUM with OD₅₉₅ = 0.05 and incubated aerobically at 37°C. The temporal profile of the PL spectra was recorded every 30 min up to 300 min to evaluate the bacterial growth-dependent sensing of the TiO₂-Cys biosensing system.

3 RESULTS AND DISCUSSION

3.1 Material Characterization of TiO₂ and TiO₂-Cys Nanoparticles

Structural analysis of TiO₂ and cysteamine-capped TiO₂ nanoparticles are shown in Figure 1A. The observed XRD pattern was compared with the standard JCPDS card [88-1172], which revealed the formation of rutile phased TiO₂ nanoparticles with tetragonal primitive lattice having lattice parameters of *a* = 4.566 Å and *c* = 2.948 Å [space group of P42/nm (136)]. The peaks at 2θ = 27.70°, 36.35°, 39.45°, 41.51°, 44.31°, 54.60°, 56.89°, 63.02°, 64.30°, 69.26°, and 70.06° correspond to (110), (101), (200), (111), (210), (211), (220), (002), (310), (301), and (112), respectively (Viana et al., 2010). The preferential plane orientation was found to be along the (110) plane for both TiO₂ and cysteamine-capped TiO₂ nanoparticles. However, cysteamine-capped TiO₂ nanoparticles showed a lesser intense diffraction plane of (110) than TiO₂, which, in turn, indicated the decreased crystallinity due to the active capping effect of cysteamine. The position of diffraction peaks corresponding to both TiO₂ and cysteamine-capped TiO₂ nanoparticles was shifted to the lower angles 2θ = ±0.2° due to the lattice mismatching, which, in turn, induce the lattice distortion.

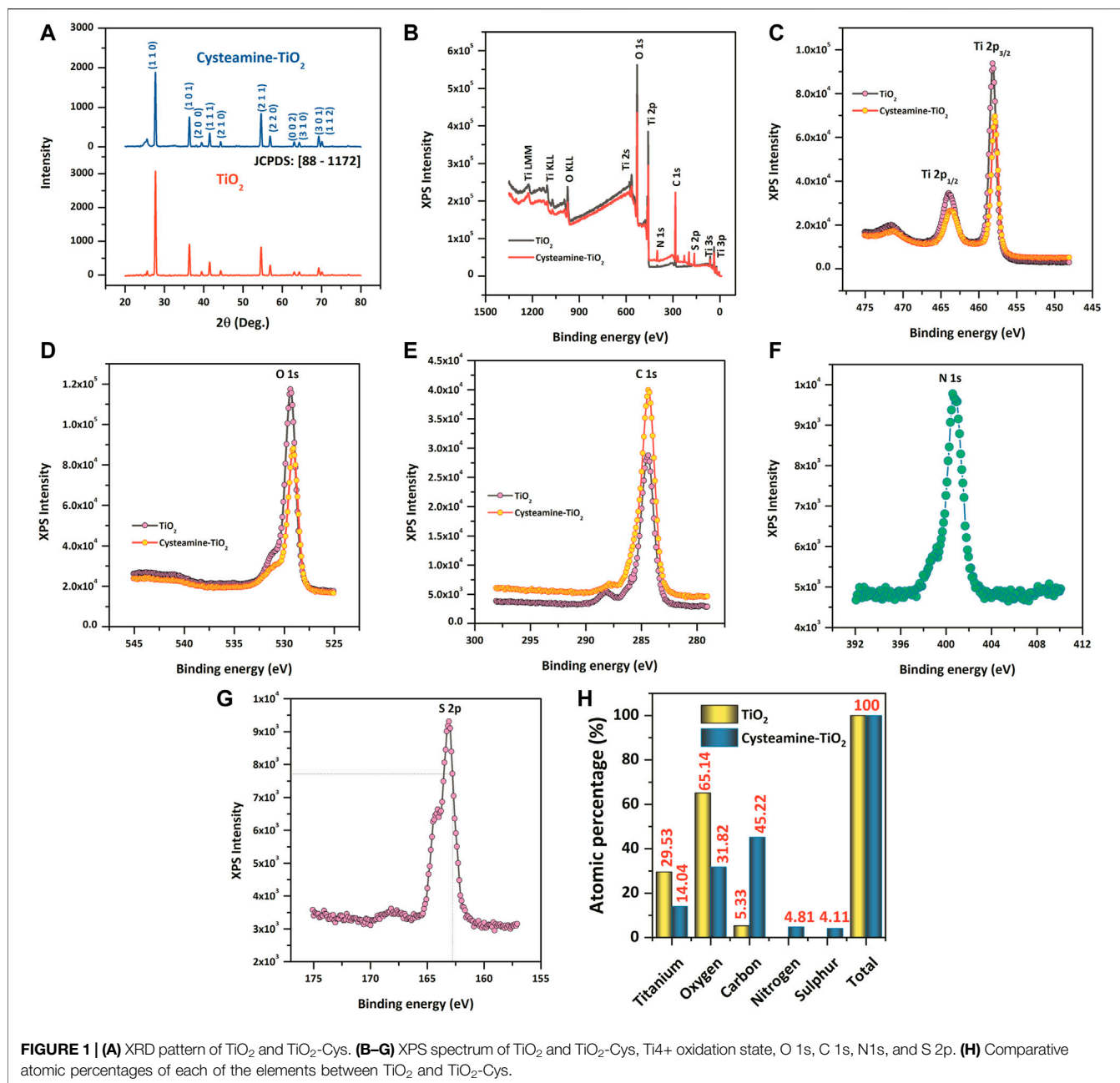


FIGURE 1 | (A) XRD pattern of TiO₂ and TiO₂-Cys. **(B–G)** XPS spectrum of TiO₂ and TiO₂-Cys, Ti⁴⁺ oxidation state, O 1s, C 1s, N 1s, and S 2p. **(H)** Comparative atomic percentages of each of the elements between TiO₂ and TiO₂-Cys.

Figure 1B displays the XPS survey spectra of TiO₂ and cysteamine-capped TiO₂ nanoparticles. The survey spectra of TiO₂ nanoparticles confirmed the existence of elements such as Ti and O, which are consistent with the previous reports. The symmetric peak having the binding energies, 465.2 and 459.5 eV, attribute to Ti 2p_{3/2} and Ti 2p_{1/2}, respectively (Hu et al., 2013; Park et al., 2015; Zhu et al., 2017). The binding energies and their difference in Ti 2p doublet of 5.8 eV confirmed the Ti⁴⁺ oxidation states (Diebold and Madey, 1996; Zhu et al., 2017). In addition, **Figure 1D** shows the peak of O 1s having a binding energy of 530.8 eV, which is in good agreement with the binding energy for TiO₂ (Diebold and Madey, 1996; Mali et al., 2012). The capping of TiO₂ by cysteamine was confirmed by the

following: a reduction in the peak intensity of Ti (**Figure 1C**) and O (**Figure 1D**) for the TiO₂-Cys, and an increase in the peak intensity of C 1s (1 (e)), N 1s (1(f)), and S 2p (1(g)) in the TiO₂-Cys. It should be noted that there were no new peaks formed, which may be due to the absence of a covalent bond between cysteamine and TiO₂ (Abbas et al., 2020). An increase in the atomic percentages of carbon (45.22%), nitrogen (4.81%), and sulfur (4.11%) was observed.

Furthermore, the morphology, size, and lattice structure were observed by TEM analysis. **Figures 2A,B** shows the TEM micrographs of TiO₂ nanoparticles and TiO₂-Cys at different magnifications. **Figure 2Ai–iv** shows the formation of nanogranular morphology of the TiO₂ nanoparticles.

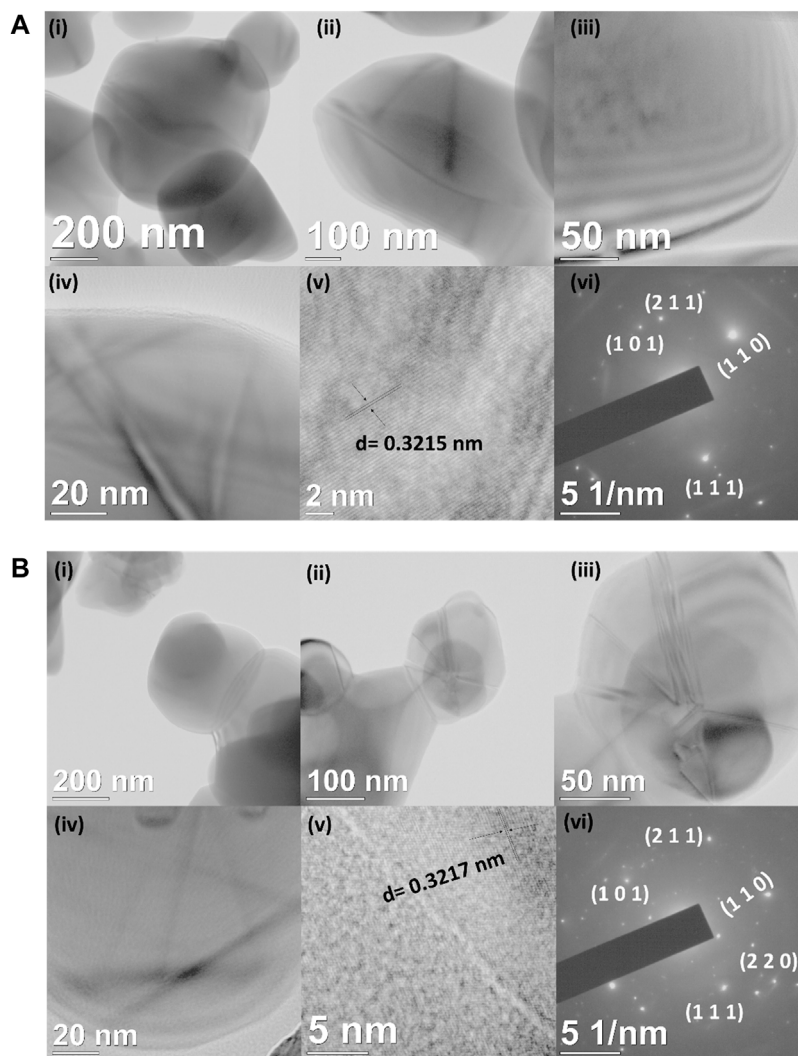


FIGURE 2 | (A) (i–iv) HR–TEM micrographs of TiO₂ nanoparticles at different magnifications. **(v)** Interplanar distance and **(vi)** SAED pattern of TiO₂ nanoparticles. **(B) (i–iv)** HR–TEM micrographs of TiO₂-Cys nanoparticles at different magnifications. **(v)** Interplanar distance and **(vi)** SAED pattern of TiO₂-Cys nanoparticles.

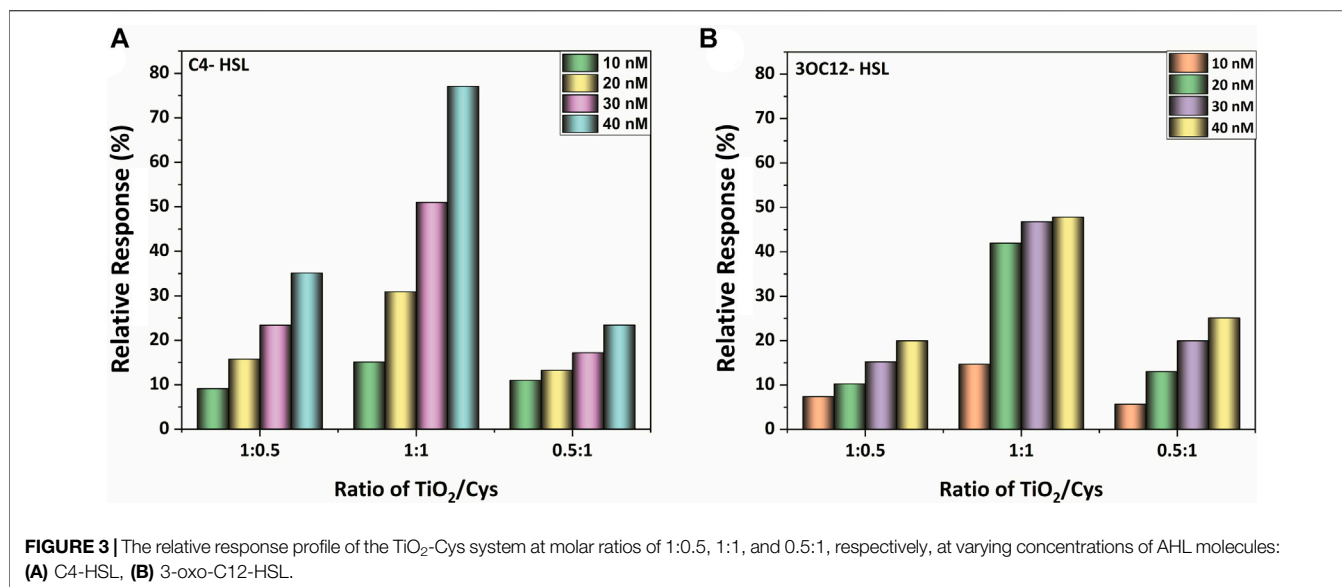
Figure 2Av shows the high-resolution TEM image representing the lattice fringe with the interplanar distance of $d = 0.321$ nm (Wang et al., 2013; Huyen et al., 2018), and the SAED (Selected Area Electron Diffraction) pattern in **Figure 2Avi** confirmed the polycrystalline nature of the synthesized TiO₂ nanoparticles. The TEM results are consistent with the XRD data. The functionalization of cysteamine is a physical attribution process in the present case, and the cysteamine molecules are highly active enough over the surface of TiO₂ nanograins. Similarly, the polycrystallinity was observed from the SAED pattern shown in **Figure 2Bvi**. Previous studies have shown the effect of calcination temperature and thus the effect of size on the optical properties of TiO₂ nanoparticles (Lin et al., 2006; Pan et al., 2013; Horti et al., 2019). At higher calcination temperatures, the size of the nanoparticles and the induced oxygen vacancies are prominent (Horti et al., 2019). A similar result is observed, at the calcination temperature of 450°C, the

average size of the TiO₂ nanoparticles obtained was ~115 nm (**Supplementary Figure S1**). The PL behavior is obtained similarly, and the oxygen vacancy (peak at 468 nm) is prominent.

3.2 Photoluminescence-Based Bioassay for AHL Detection

3.2.1 Optimization of TiO₂-Cys ratio for AHL Response

From the structural characterization methods, capping of the cysteamine around TiO₂ nanoparticles is evident. Furthermore, to evaluate the maximum biosensing outcome, the PL spectrum was observed for the three different molar ratios of TiO₂-Cys (0.5:1, 1:1, and 1:0.5). **Figures 3A,B** show the relative response profile of the various ratios for the increasing concentrations (10–40 nM) of the bioanalyte, C4-HSL, and 3-Oxo-C12 HSL, respectively. The results demonstrated that 1:1 is the optimal ratio of the TiO₂-Cys for both the AHLs considered. The relative



response was dependent on the concentration of AHL molecules, with a maximum value of 80% obtained for C4-HSL. At this ratio, the optimal exposure of the defect centers to cysteamine was achieved, which significantly improved the relative response of the biosensing system. A similar trend was previously reported for ZnO-Cys (Tavakkoli Yarakhi et al., 2017; Vasudevan et al., 2020). While the concentration of cysteamine was less, it was not sufficient to interact with the defect centers of the TiO₂ nanoparticles and, in turn, was insufficient to detect the AHL molecules, leading to the decreased relative response. On the other hand, when the cysteamine concentration exceeds the TiO₂ nanoparticles, the reduced relative response was due to the interaction of cysteamine with most of the defect centers. Hence, upon the addition of AHL molecules, the presence of excessive cysteamine led to a reduced relative response. Thus, for further studies, a 1:1 ratio of TiO₂-Cys was considered.

3.2.2 Spectral Profile of TiO₂-Cys Towards AHL Detection

Figure 4 depicts the PL spectral defect profile of the synthesized TiO₂ nanoparticles excited at the wavelength of 320 nm. It is known that the PL behavior is different for the anatase and the rutile phase (Pallotti et al., 2017). The XRD analysis of the current study reported that the TiO₂ nanoparticles is in its rutile phase. Even though the exact mechanism of the rutile PL spectrum is poorly understood, several researchers explain two hypotheses: free holes mechanism (Knorr et al., 2008; Rex et al., 2016) and trapped holes (Nakamura and Nakato, 2004; Nakamura et al., 2005) mechanism. A recent report decoded the rutile PL mechanism and claimed that recombination of free carriers with the valence band holes initiates the rutile PL where the enhancement of PL is caused by the O₂ adsorption (Pallotti et al., 2017).

Considering the current study, the following intrinsic defect states were obtained as excitation peaks in the PL spectrum: 424, 468, 484, and 493 nm. The peak at 424 nm is due to the self-

trapped excitons (STE) of the TiO₆²⁻ octahedron and the recombination of free excitons. This is generated by the lattice localized electron upon the excitation at 320 nm, which captures a hole (Rathore et al., 2021). The emission peak at 468 nm, equivalent to 2.65 eV, is attributed to the surface oxygen vacancies and defects (Akshay et al., 2019b; Rathore et al., 2021). While the peak at 484 nm is due to the blue-green emission band that is attributed to the de-excitation to acceptor surface defects (Prajapati et al., 2017; Akshay et al., 2019a), the peak at 491 nm is due to the charge transition associated with oxygen defects (Choudhury and Choudhury, 2014). Among the observed peaks, the peak at 468 nm of surface oxygen vacancies and defects accounted for the AHL detection, due to its prominence over the other peaks. Figures 4A,B depict the PL spectrum recorded for the TiO₂, Cysteamine-capped TiO₂ and TiO₂-Cys in the presence of an increasing concentration of the AHL molecules. The studies tested the detection of the AHL molecules: C4-HSL and 3-Oxo-C12 HSL molecules, which are indigenously produced by the pathogen *P. aeruginosa*. It should be noted that the capping of TiO₂ nanoparticles by cysteamine has significantly quenched the luminescence of TiO₂, possibly masking the oxygen defect centers. However, upon the addition of AHL, there was a concentration-dependent increase in the intensity of peak at 468 nm observed in the spectral profile. As previously proven for the ZnO-Cys system (Vasudevan et al., 2020), the carbonyl group of AHL and the amine group of the cysteamine possibly interact. This exposes the defect centers of TiO₂, thereby increasing the PL emission intensity by adding the AHL molecules. To ensure that free cysteamine does not interfere with the sensing process, PL was recorded at the same conditions at different concentrations of C4-HSL (Supplementary Figure S2). It was observed that there was no peak at 468 nm detected, in the given excitation wavelength. This confirms that no interfering effect is observed in the response of the developed bioassay because of the free ligands.

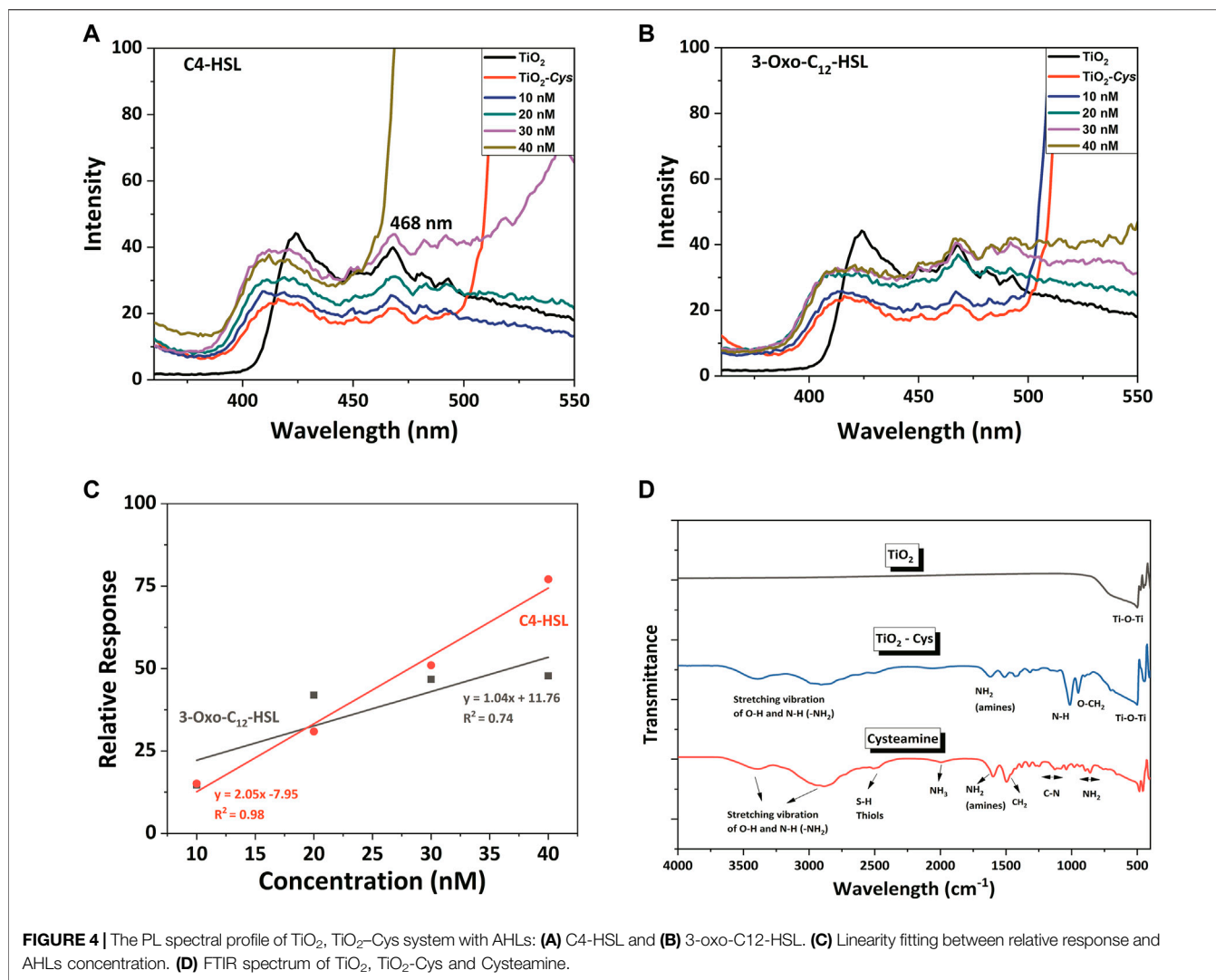


FIGURE 4 | The PL spectral profile of TiO₂, TiO₂-Cys system with AHLs: **(A)** C4-HSL and **(B)** 3-oxo-C₁₂-HSL. **(C)** Linearity fitting between relative response and AHLs concentration. **(D)** FTIR spectrum of TiO₂, TiO₂-Cys and Cysteamine.

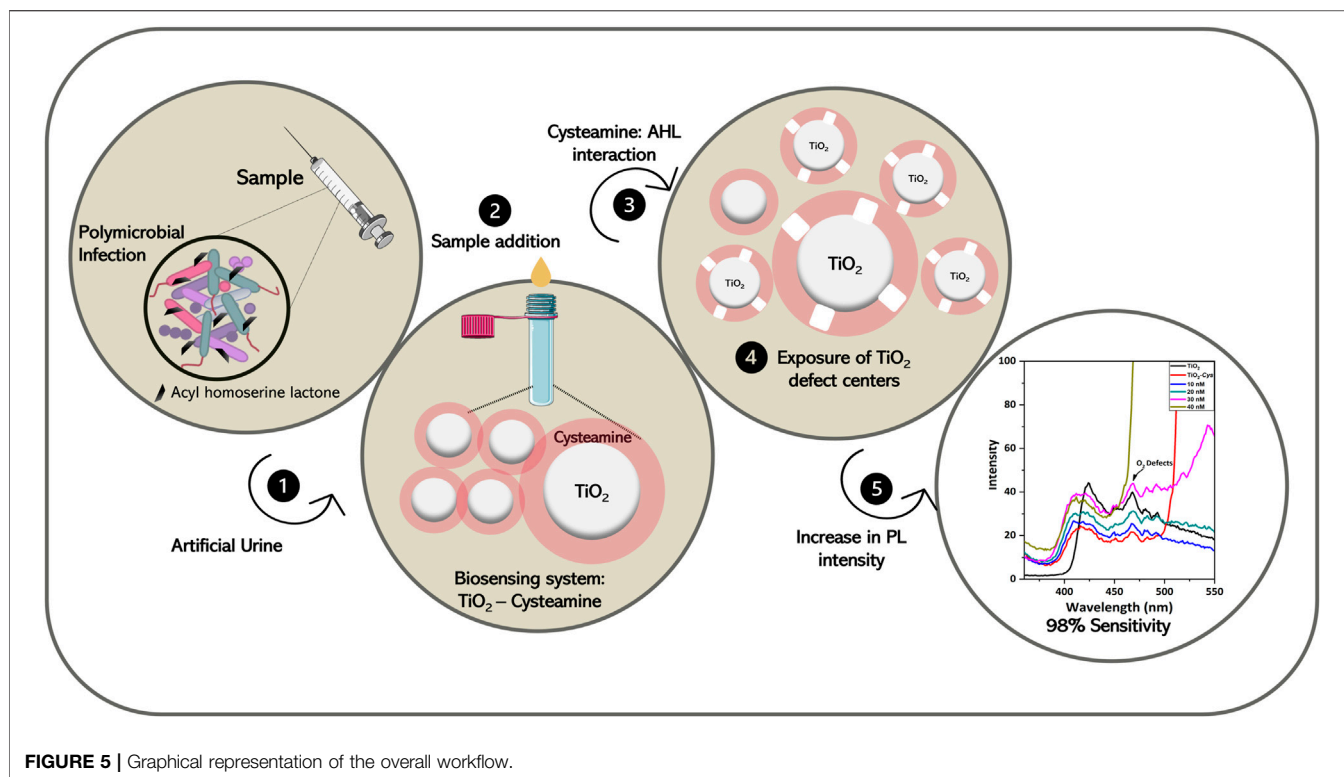
Among the two AHLs considered, C4 -HSL showed a higher relative response than 3-Oxo-C₁₂. The only structural difference between the two AHLs is the carbon chain length and associated hydrophobicity. Thus, the PL intensity is shown to be sensitive to the hydrophobicity of the AHL molecules. The varying concentrations of AHL molecules from 10 to 40 nM were taken for the sensing studies. In general, adding AHL molecules increased the intensity of the 468-nm peak in a concentration-dependent manner. In particular, the C4-HSL exhibited increased intensity at the concentration greater than 30 nM compared to TiO₂ and TiO₂-Cys. However, the 3-Oxo-C₁₂ HSL showed a marginal increase of PL intensity at a concentration above 30 nM that of the TiO₂ but more than that of TiO₂-Cys. A similar trend was observed for the ZnO-Cys, which proves the role of the AHL carbon chain in determining the interaction between the amine group of cysteamine and AHL molecules. The linear relationship between the relative response and the AHL concentration was linearly fit in the following equations:

$$\text{C4 - HSL} : y = 2.05x - 7.95, R^2 = 0.98 \quad (2)$$

$$\text{3-oxo-C}_{12}\text{HSL} : y = 1.04x + 11.76, R^2 = 0.74 \quad (3)$$

In the case of C4-HSL, the R^2 approaching 0.98 very well establishes the linear relationship between the relative response and the AHL concentration. In the previous study with ZnO-Cys, the linearity of the biosensing system was proven for all the AHL molecules considered, despite reduced relative response in the case of long-chain AHL molecules. A similar result was obtained for the current case with TiO₂-Cys where it is highly linear for short-chain AHL molecules and comparatively less linear in the case of long-chain AHL molecule considered.

The interaction of TiO₂ and cysteamine was decoded by observing the FTIR spectrum (**Figure 4D**). The O-Ti-O functional group was proved from the characteristic peak at 503 cm⁻¹ for TiO₂ and TiO₂-Cys (Erdem et al., 2001; Padmanabhan et al., 2007; Zhang et al., 2018). The presence of cysteamine was confirmed by thiol and amines (NH₂), having peaks at 2,499 and 1,600 cm⁻¹, respectively (Vasudevan et al., 2020). As



observed in our previous report, the peak corresponding to the S-H thiol group was absent in the case of the TiO₂-Cys system, which confirmed the capping effect of TiO₂ by cysteamine through thiol linkages. This also supported the optimal ratio of 1:1 of TiO₂-Cys. Another point to be noted is the presence of the NH₂ group in the TiO₂-Cys, which is proven to have strong interaction with the carbonyl group. Thus, like the ZnO-Cys system, the TiO₂-Cys system interacts with each other through the thiol group, exposing the amine functional group. This possibly facilitates the interaction of the amine group with the carbonyl chain of the AHL molecule leading to the enhanced PL intensity at 468 nm. It should be noted that the presence of the amine functional group is not prominent as observed previously for the ZnO-Cys system. This is possibly due to the dominance of electrostatic interactions between TiO₂ and cysteamine as reported previously (Park, 2011). TiO₂ has an isoelectric point of 5.8 (McNamee et al., 2005) which has a strong electrostatic interaction with cysteamine having an isoelectric point of 9.5 (Ma et al., 2020). Thus, it is evident that the isoelectric points play a role in the enhanced electrostatic interaction between cysteamine and TiO₂. Thus, the combination of thiol linkage and electrostatic interactions facilitates the stable capping of cysteamine. **Figure 5** depicts the graphical representation of the biosensing mechanism.

3.2.3 Spectral Profile of TiO₂-Cys Towards AHL Detection in Simulated Host Environment: Artificial Urine Media

The relative response and the selectivity of TiO₂-Cys were further evaluated in the presence of a simulated host

environment—AUM. AUM was prepared (**Supplementary Table S1**) as previously reported by Brooks and Keevil (1997). This study evaluates the selectivity of the sensing system in the presence of possible interference molecules. pH is the important factor that differentiates the healthy and the diseased condition (Lai et al., 2019). It was shown that for complicated urinary tract infections, pH moves towards the alkaline zone, whereas for uncomplicated UTI, the pH is almost maintained neutral (Yaxley, 2016). The reported composition of AUM was stable at pH 6.5, and upon an increase in pH, salts precipitate, leading to an unstable condition (Brooks and Keevil, 1997). However, to account for the relative response of the developed biosensing system concerning the varying pH, AUM was prepared at different pH—6.5, 7, and 8. The relative response profile was measured at a concentration of 160 nM. This concentration was chosen since C4-HSL and 3-oxo-C12 HSL exhibited maximum relative response at 160 nM in the AUM medium (pH 6.5).

Figure 6A shows that the biosensing system TiO₂-Cys provided a stable response in the simulated host environment at pH 6.5. As expected, the maximum relative response for C4-HSL and 3-Oxo-C12 HSL was obtained at AUM having pH 6.5. There was a decreasing trend in the relative response of the biosensing system as the pH increased. The precipitation of salts at the increased pH is possible for this trend (Brooks and Keevil, 1997). Also, the previous study proved that the electrostatic interaction between TiO₂ and cysteamine is dependent on the pH largely (Park, 2011). Thus, in addition to the AUM stability at pH 6.5, the electrostatic interactions between TiO₂ and cysteamine contributed to the enhanced interaction with the AHL molecule at the pH of 6.5. The relative response of the

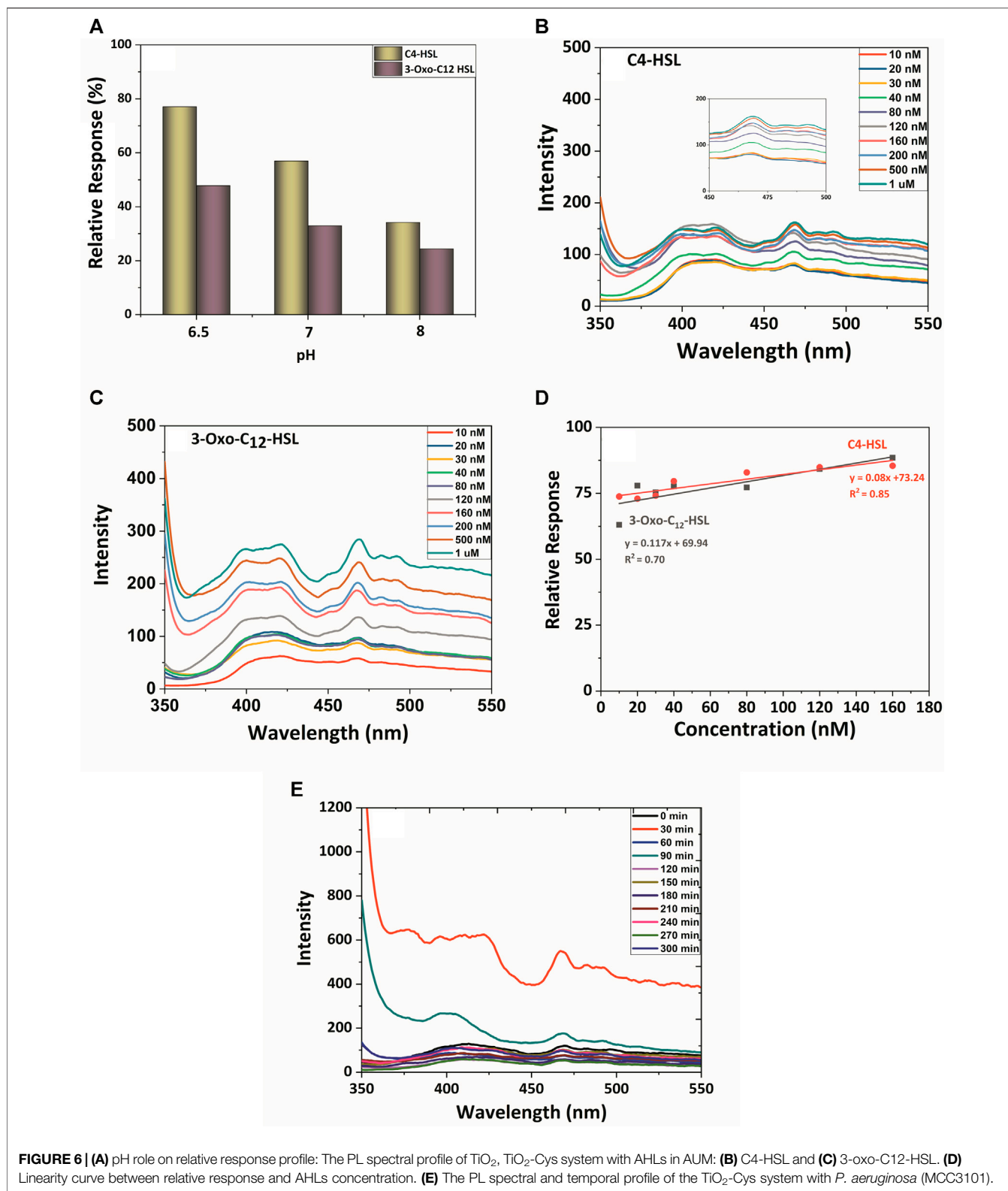


FIGURE 6 | (A) pH role on relative response profile: The PL spectral profile of TiO₂, TiO₂-Cys system with AHLs in AUM: **(B)** C4-HSL and **(C)** 3-oxo-C12-HSL. **(D)** Linearity curve between relative response and AHLs concentration. **(E)** The PL spectral and temporal profile of the TiO₂-Cys system with *P. aeruginosa* (MCC3101).

biosensing system in varying pH needs further studies on the actual urine samples.

At the stable pH 6.5 of AUM, the PL spectrum profile was measured for the TiO₂-Cys biosensing system (**Figures**

6B,C). This study also accounted for the performance of the biosensing system in the presence of possible interferences in the host environment, including salts, metals, and other components. The spectrum profile

highlighted the signature peak of 468 nm in AUM. In the AUM environment, carbon-chain length and associated hydrophobicity played an important role in the specificity of the system (**Figure 6D**). The response recorded for C4-HSL was more profound when compared to the long-chain AHL, 3-Oxo-C12 HSL. Upon increasing concentrations from 10 nM to 1 μM, there was an increase in PL intensity. A closer look in the relative response by fitting the linear response (**Eqs 4, 5**) between the concentration and relative response revealed that the biosensing system attained maximum relative response at 160 nM, which led to the saturation in the response:

$$\text{C4-HSL: } y = 0.08x + 73.24, R^2 = 0.85 \quad (4)$$

$$\text{3-oxo-C}_{12}\text{HSL: } y = 0.117x + 69.94, R^2 = 0.70 \quad (5)$$

The reduction in the linearity (R^2) is possibly due to the stability of AUM at pH 6.5. Even then, linear response with R^2 values 0.85 was observed for C4-HSL, and a slight reduction in 3-oxo-C12 was observed having an R^2 value of 0.7.

3.2.4 Real-Time Biosensing Profile

The robustness of the biosensing system was validated by measuring the PL response with *P. aeruginosa*, which naturally produces two AHL molecules: C4-HSL and 3-Oxo-C12 HSL in a time-dependent manner. It should also be noted that the *Pseudomonas* sp. is known to produce several secondary metabolites, besides the AHL molecules (Gross and Loper, 2009). The real-time profiling also validates the selectivity of the sensing system in the presence of these secondary metabolites and the urine components.

P. aeruginosa (MCC 3101), a model micro-organism, was inoculated in AUM, and the response of the biosensing system was measured for every 30 min till 5 h (**Figure 6E**). The release and accumulation of AHL molecules are density-dependent; i.e., the increase in the number of cells increases the AHL molecules accumulation (Papenfort and Bassler, 2016). The TiO₂-Cys system sensed the AHL molecules released by the bacteria with the maximum intensity of 468 nm peak at the time point of 30 min. While a time-dependent linear response was foreseen, the peak intensity was decreased after 30 min, itself. This was due to the inherently dynamic nature of the biological system. The released AHL molecules are primarily and most specifically detected by the bacterial quorum sensing receptors to activate QS (Papenfort and Bassler, 2016). This leaves the undetected molecules available for our biosensing system to detect. Hence, there was a possible decrease in the peak intensity in the later time points. However, this might not be the case in real conditions. The polymicrobial environment having bacterial species that produced other different AHL molecules will also be present along with the considered AHL molecules. Thus, further studies on different AHL-producing strains and in different host-simulated environments are being carried out to elaborate the specificity and sensitivity of the TiO₂-Cys biosensing system to detect AHL molecules and thereby diagnose infections effectively.

4 CONCLUSION

The alarming increase in life-threatening infections necessitates the growing need for immediate infection diagnosis. This requires the advent of point-of-care diagnostics that are rapid and non-invasive with minimal or no sample processing. In this regard, this is the first study to report the bioassay based on cysteamine-capped TiO₂ nanoparticles to identify the quorum sensing signaling molecule, AHL. The characterization analysis revealed the capping of cysteamine around TiO₂ nanoparticles. This capping by cysteamine quenches the TiO₂ photoluminescence. The external addition of AHL unmasks the oxygen defect states and thereby enhancing the PL intensity at 468 nm. The highlighting aspect of the study is that the selectivity and the specificity of the bioassay were proven in the host simulated condition—AUM. Through this study, the role of oxygen vacancies is well established in AHL sensing. The host sensing environment and difference in the isoelectric point determine the choice of metal oxide nanostructures and the linker molecule. The lesser the difference between isoelectric points, the more the relative response for AHL detection. Further studies are in progress to explore metal oxides, different linker molecules with varying isoelectric points, electronic bandgaps, and strong evidence of interaction between cysteamine and interface materials.

DATA AVAILABILITY STATEMENT

The original contributions presented in the study are included in the article/**Supplementary Material**. Further inquiries can be directed to the corresponding authors.

AUTHOR CONTRIBUTIONS

SV and PS—Formal Analysis, Investigation, Visualization, Data Curation, and Writing—Original Draft. APS, JBB, and PN—Conceptualization, Methodology, Supervision, Resources, Writing—Review and Editing, and Project Administration.

ACKNOWLEDGMENTS

SV wishes to express her gratitude to SASTRA Deemed to be University for providing her an opportunity to carry out the present work as part of her Ph.D dissertation work and DST-INSPIRE (IF170369) for the financial support. All authors extend their sincere gratitude to FIST Scheme of Department of Science & Technology (SR/FST/ET-II/2018/221) for the financial support.

SUPPLEMENTARY MATERIAL

The Supplementary Material for this article can be found online at: <https://www.frontiersin.org/articles/10.3389/fbioe.2021.750933/full#supplementary-material>

REFERENCES

- Abbas, S. S., Kelly, N. L., Patias, G., Hanna, J. V., and McNally, T. (2020). Cysteamine Functionalised Reduced Graphene Oxide Modification of Maleated Poly(propylene). *Polymer* 203, 122750. doi:10.1016/j.polymer.2020.122750
- Akshay, V. R., Arun, B., Mandal, G., Chanda, A., and Vasundhara, M. (2019a). Significant Reduction in the Optical Band-gap and Defect Assisted Magnetic Response in Fe-Doped Anatase TiO₂ Nanocrystals as Dilute Magnetic Semiconductors. *New J. Chem.* 43, 6048–6062. doi:10.1039/C9NJ00275H
- Akshay, V. R., Arun, B., Mandal, G., and Vasundhara, M. (2019b). Visible Range Optical Absorption, Urbach Energy Estimation and Paramagnetic Response in Cr-Doped TiO₂ Nanocrystals Derived by a Sol-Gel Method. *Phys. Chem. Chem. Phys.* 21, 12991–13004. doi:10.1039/C9CP01351B
- Azimi, S., Klementiev, A. D., Whiteley, M., and Diggle, S. P. (2020). Bacterial Quorum Sensing during Infection. *Annu. Rev. Microbiol.* 74, 201–219. doi:10.1146/annurev-micro-032020-093845
- Brooks, T., and Keevil, C. W. (1997). A Simple Artificial Urine for the Growth of Urinary Pathogens. *Letts. Appl. Microbiol.* 24, 203–206. doi:10.1046/j.1472-765X.1997.00378.x
- Chahande, A. M., Lathigara, D., Prabhune, A. A., and Devi, R. N. (2021). Red Fluorescent Ultra-small Gold Nanoclusters Functionalized with Signal Molecules to Probe Specificity in Quorum Sensing Receptors in Gram-Negative Bacteria. *Arch. Microbiol.* 203, 4293–4301. doi:10.1007/s00203-021-02338-y
- Choudhury, B., and Choudhury, A. (2014). Oxygen Defect Dependent Variation of Band gap, Urbach Energy and Luminescence Property of Anatase, Anatase-Rutile Mixed Phase and of Rutile Phases of TiO₂ Nanoparticles. *Physica E: Low-dimensional Syst. Nanostructures* 56, 364–371. doi:10.1016/j.physe.2013.10.014
- Diebold, U., and Madey, T. E. (1996). TiO₂ by XPS. *Surf. Sci. Spectra* 4, 227–231. doi:10.1116/1.1247794
- Ensaifi, A. A., Sohrabi, M., Jafari-Asl, M., and Rezaei, B. (2015). Selective and Sensitive Furazolidone Biosensor Based on DNA-Modified TiO₂-reduced Graphene Oxide. *Appl. Surf. Sci.* 356, 301–307. doi:10.1016/j.apsusc.2015.08.085
- Erdem, B., Hunsicker, R. A., Simmons, G. W., Sudol, E. D., Dimonie, V. L., and El-Aasser, M. S. (2001). XPS and FTIR Surface Characterization of TiO₂ Particles Used in Polymer Encapsulation. *Langmuir* 17, 2664–2669. doi:10.1021/la0015213
- Gross, H., and Loper, J. E. (2009). Genomics of Secondary Metabolite Production by *Pseudomonas* Spp. *Nat. Prod. Rep.* 26, 1408–1446. doi:10.1039/b817075b
- Habimana, J. d. D., Ji, J., Pi, F., Karangwa, E., Sun, J., Guo, W., et al. (2018). A Class-specific Artificial Receptor-Based on Molecularly Imprinted Polymer-Coated Quantum Dot Centers for the Detection of Signaling Molecules, N-Acyl-Homoserine Lactones Present in Gram-Negative Bacteria. *Analytica Chim. Acta* 1031, 134–144. doi:10.1016/j.aca.2018.05.018
- Haider, A. J., Jameel, Z. N., and Al-Hussaini, I. H. M. (2019). Review on: Titanium Dioxide Applications. *Energ. Proced.* 157, 17–29. doi:10.1016/j.egypro.2018.11.159
- Horti, N. C., Kamatagi, M. D., Patil, N. R., Nataraj, S. K., Sannaikar, M. S., and Inamdar, S. R. (2019). Synthesis and Photoluminescence Properties of Titanium Oxide (TiO₂) Nanoparticles: Effect of Calcination Temperature. *Optik* 194, 163070. doi:10.1016/j.jlloe.2019.163070
- Hu, W., Liu, Y., Withers, R. L., Frankcombe, T. J., Norén, L., Snashall, A., et al. (2013). Electron-pinned Defect-Dipoles for High-Performance Colossal Permittivity Materials. *Nat. Mater* 12, 821–826. doi:10.1038/nmat3691
- Huyen, T., Chi, T., Dung, N., Kosslick, H., and Liem, N. (2018). Enhanced Photocatalytic Activity of {110}-Faceted TiO₂ Rutile Nanorods in the Photodegradation of Hazardous Pharmaceuticals. *Nanomaterials* 8, 276. doi:10.3390/nano8050276
- Jiang, H., Jiang, D., Shao, J., and Sun, X. (2016). Magnetic Molecularly Imprinted Polymer Nanoparticles Based Electrochemical Sensor for the Measurement of Gram-Negative Bacterial Quorum Signaling Molecules (N-Acyl-Homoserine-Lactones). *Biosens. Bioelectron.* 75, 411–419. doi:10.1016/j.bios.2015.07.045
- Jo, N. r., and Shin, Y.-B. (2020). Enhancing Biosensing Sensitivity of Metal Nanostructures through Site-Selective Binding. *Sci. Rep.* 10, 1–7. doi:10.1038/s41598-020-57791-4
- Kang, X., Liu, S., Dai, Z., He, Y., Song, X., and Tan, Z. (2019). Titanium Dioxide: From Engineering to Applications. *Catalysts* 9, 191. doi:10.3390/catal9020191
- Kawaguchi, T., Chen, Y. P., Norman, R. S., and Decho, W. A. (2008). Rapid Screening of Quorum-Sensing Signal N-Acyl Homoserine Lactones by an *In Vitro* Cell-free Assay. *Appl. Environ. Microbiol.* 74, 3667–3671. doi:10.1128/AEM.02869-07
- Klockgether, J., and Tümmler, B. (2017). Recent Advances in Understanding *Pseudomonas aeruginosa* as a Pathogen. *F1000Res* 6, 1261. doi:10.12688/f1000research.10506.1
- Knorr, F. J., Mercado, C. C., and McHale, J. L. (2008). Trap-State Distributions and Carrier Transport in Pure and Mixed-phase TiO₂: Influence of Contacting Solvent and Interphasic Electron Transfer. *J. Phys. Chem. C* 112, 12786–12794. doi:10.1021/jp8039934
- Kumari, A., Pasini, P., and Daunert, S. (2008). Detection of Bacterial Quorum Sensing N-Acyl Homoserine Lactones in Clinical Samples. *Anal. Bioanal. Chem.* 391, 1619–1627. doi:10.1007/s00216-008-2002-3
- Lai, H.-C., Chang, S.-N., Lin, H.-C., Hsu, Y.-L., Wei, H.-M., Kuo, C.-C., et al. (2021). Association between Urine pH and Common Uropathogens in Children with Urinary Tract Infections. *J. Microbiol. Immunol. Infect.* 54, 290–298. doi:10.1016/j.jmii.2019.08.002
- Lee, J., and Zhang, L. (2015). The Hierarchy Quorum Sensing Network in *Pseudomonas aeruginosa*. *Protein Cell* 6, 26–41. doi:10.1007/s13238-014-0100-x
- Lin, H., Huang, C., Li, W., Ni, C., Shah, S., and Tseng, Y. (2006). Size Dependency of Nanocrystalline TiO₂ on its Optical Property and Photocatalytic Reactivity Exemplified by 2-chlorophenol. *Appl. Catal. B: Environ.* 68, 1–11. doi:10.1016/j.apcatb.2006.07.018
- Ma, Q., Fang, X., Zhang, J., Zhu, L., Rao, X., Lu, Q., et al. (2020). Discrimination of Cysteamine from Mercapto Amino Acids through Isoelectric point-mediated Surface Ligand Exchange of β -cyclodextrin-modified Gold Nanoparticles. *J. Mater. Chem. B* 8, 4039–4045. doi:10.1039/d0tb00462f
- Mali, S. S., Betty, C. A., Bhosale, P. N., and Patil, P. S. (2012). Synthesis, Characterization of Hydrothermally Grown MWCNT-TiO₂ Photoelectrodes and Their Visible Light Absorption Properties. *ECS J. Solid State. Sci. Technol.* 1, M15–M23. doi:10.1149/2.004202jss
- Marsalek, R. (2014). Particle Size and Zeta Potential of ZnO. *APCBEE Proced.* 9, 13–17. doi:10.1016/j.apcbee.2014.01.003
- McNamee, C. E., Tsujii, Y., and Matsumoto, M. (2005). Physicochemical Characterization of an Anatase TiO₂ Surface and the Adsorption of a Nonionic Surfactant: An Atomic Force Microscopy Study. *Langmuir* 21, 11283–11288. doi:10.1021/la0517890
- Mittal, R., Aggarwal, S., Sharma, S., Chhibber, S., and Harjai, K. (2009). Urinary Tract Infections Caused by *Pseudomonas aeruginosa*: A Minireview. *J. Infect. Public Health* 2, 101–111. doi:10.1016/j.jiph.2009.08.003
- Mukherji, R., Samanta, A., Illathvalappil, R., Chowdhury, S., Prabhune, A., and Devi, R. N. (2013). Selective imaging of Quorum sensing receptors in bacteria using fluorescent au nanocluster probes surface functionalized with signal molecules. *ACS Appl. Mater. Inter.* 5, 13076–13081. doi:10.1021/am404093m
- Muras, A., Otero-Casal, P., Blanc, V., and Otero, A. (2020). Acyl Homoserine Lactone-Mediated Quorum Sensing in the Oral Cavity: a Paradigm Revisited. *Sci. Rep.* 10, 1–14. doi:10.1038/s41598-020-66704-4
- Nakamura, R., and Nakato, Y. (2004). Primary Intermediates of Oxygen Photoevolution Reaction on TiO₂ (Rutile) Particles, Revealed by *In Situ* FTIR Absorption and Photoluminescence Measurements. *J. Am. Chem. Soc.* 126, 1290–1298. doi:10.1021/ja0388764
- Nakamura, R., Okamura, T., Ohashi, N., Imanishi, A., and Nakato, Y. (2005). Molecular Mechanisms of Photoinduced Oxygen Evolution, PL Emission, and Surface Roughening at Atomically Smooth (110) and (100) N-TiO₂ (Rutile) Surfaces in Aqueous Acidic Solutions. *J. Am. Chem. Soc.* 127, 12975–12983. doi:10.1021/ja053252e
- Oliva, J. M., Ríos de la Rosa, J. M., Sayagués, M. J., Sánchez-Alcázar, J. A., Merklings, P. J., and Zaderenko, A. P. (2018). Solvent-assisted *In Situ* Synthesis of Cysteamine-Capped Silver Nanoparticles. *Adv. Nat. Sci. Nanosci. Nanotechnol.* 9, 015001. doi:10.1088/2043-6254/aa9de9
- Padmanabhan, S. C., Pillai, S. C., Colreavy, J., Balakrishnan, S., McCormack, D. E., Perova, T. S., et al. (2007). A Simple Sol-Gel Processing for the Development of High-Temperature Stable Photoactive Anatase Titania. *Chem. Mater.* 19, 4474–4481. doi:10.1021/cm070980n

- Pallotti, D. K., Passoni, L., Maddalena, P., Di Fonzo, F., and Lettieri, S. (2017). Photoluminescence Mechanisms in Anatase and Rutile TiO₂. *J. Phys. Chem. C* 121, 9011–9021. doi:10.1021/acs.jpcc.7b00321
- Pan, X., Yang, M.-Q., Fu, X., Zhang, N., and Xu, Y.-J. (2013). Defective TiO₂ with Oxygen Vacancies: Synthesis, Properties and Photocatalytic Applications. *Nanoscale* 5, 3601–3614. doi:10.1039/C3NR00476G
- Papenfert, K., and Bassler, B. L. (2016). Quorum sensing Signal-Response Systems in Gram-Negative Bacteria. *Nat. Rev. Microbiol.* 14, 576–588. doi:10.1038/nrmicro.2016.89
- Park, J.-W. (2011). Effect of Cysteamine Layer Formed on Gold Surfaces Interacting with TiO₂ Surfaces. *Curr. Appl. Phys.* 11, 498–502. doi:10.1016/j.cap.2010.09.001
- Park, J., Back, T., Mitchel, W. C., Kim, S. S., Elhamri, S., Boeckl, J., et al. (2015). Approach to Multifunctional Device Platform with Epitaxial Graphene on Transition Metal Oxide. *Sci. Rep.* 5, 14374. doi:10.1038/srep14374
- Prajapati, B., Kumar, S., Kumar, M., Chatterjee, S., and Ghosh, A. K. (2017). Investigation of the Physical Properties of Fe:TiO₂-Diluted Magnetic Semiconductor Nanoparticles. *J. Mater. Chem. C* 5, 4257–4267. doi:10.1039/C7TC00233E
- Rathore, N., Kulshreshtha, A., Shukla, R. K., and Sharma, D. (2021). Optical, Structural and Morphological Properties of Fe Substituted Rutile Phase TiO₂ Nanoparticles. *Physica B: Condensed Matter* 600, 412609. doi:10.1016/j.physb.2020.412609
- Rex, R. E., Yang, Y., Knorr, F. J., Zhang, J. Z., Li, Y., and McHale, J. L. (2016). Spectroelectrochemical Photoluminescence of Trap States in H-Treated Rutile TiO₂ Nanowires: Implications for Photooxidation of Water. *J. Phys. Chem. C* 120, 3530–3541. doi:10.1021/acs.jpcc.5b11231
- Rutherford, S. T., and Bassler, B. L. (2012). Bacterial Quorum Sensing: its Role in Virulence and Possibilities for its Control. *Cold Spring Harbor Perspect. Med.* 2, a012427. doi:10.1101/cshperspect.a012427
- Schuster, M., Lostroh, C. P., Ogi, T., and Greenberg, E. P. (2003). Identification, Timing, and Signal Specificity of *Pseudomonas aeruginosa* Quorum-controlled Genes: a Transcriptome Analysis. *J. Bacteriol.* 185, 2066–2079. doi:10.1128/jb.185.7.2066-2079.2003
- Sharon, M. (2014). Surface Orchestration of Gold Nanoparticles Using Cysteamine as Linker and Folate as Navigating Molecule for Synaptic Delivery of Doxorubicin. *jnmr* 1. doi:10.15406/jnmr.2014.01.00002
- Solanki, P. R., Kaushik, A., Agrawal, V. V., and Malhotra, B. D. (2011). Nanostructured Metal Oxide-Based Biosensors. *NPG Asia Mater.* 3, 17–24. doi:10.1038/asiamat.2010.137
- Steindler, L., and Venturi, V. (2007). Detection of Quorum-sensing N-acyl Homoserine Lactone Signal Molecules by Bacterial Biosensors. *FEMS Microbiol. Lett.* 266, 1–9. doi:10.1111/j.1574-6968.2006.00501.x
- Struss, A., Pasini, P., Ensor, C. M., Raut, N., and Daunert, S. (2010). Paper Strip Whole Cell Biosensors: a Portable Test for the Semiquantitative Detection of Bacterial Quorum Signaling Molecules. *Anal. Chem.* 82, 4457–4463. doi:10.1021/ac100231a
- Subramoni, S., and Venturi, V. (2009). LuxR-family 'solos': Bachelor Sensors/regulators of Signalling Molecules. *Microbiology* 155, 1377–1385. doi:10.1099/mic.0.026849-0
- Tavakkoli Yarak, M., Tayebi, M., Ahmadi, M., Tahriri, M., Vashae, D., and Tayebi, L. (2017). Synthesis and Optical Properties of Cysteamine-Capped ZnS Quantum Dots for Aflatoxin Quantification. *J. Alloys Compounds* 690, 749–758. doi:10.1016/j.jallcom.2016.08.158
- Tayebi, M., Tavakkoli Yarak, M., Ahmadi, M., Tahriri, M., Vashae, D., and Tayebi, L. (2016). Determination of Total Aflatoxin Using Cysteamine-Capped CdS Quantum Dots as a Fluorescence Probe. *Colloid Polym. Sci.* 294, 1453–1462. doi:10.1007/s00396-016-3903-x
- Tuon, F. F., Gortz, L. W., and Rocha, J. L. (2012). Risk Factors for Pan-Resistant *Pseudomonas aeruginosa* Bacteremia and the Adequacy of Antibiotic Therapy. *Braz. J. Infect. Dis.* 16, 351–356. doi:10.1016/j.bjid.2012.06.009
- Vasudevan, S., Srinivasan, P., Rayappan, J. B. B., and Solomon, A. P. (2020). A Photoluminescence Biosensor for the Detection of N-Acyl Homoserine Lactone Using Cysteamine Functionalized ZnO Nanoparticles for the Early Diagnosis of Urinary Tract Infections. *J. Mater. Chem. B* 8, 4228–4236. doi:10.1039/c9tb02243k
- Venkataprasad, G., Madhusudana Reddy, T., Lakshmi Narayana, A., Hussain, O. M., Venu Gopal, T., and Shaikshavali, P. (2020). Hydrothermal Synthesis of Intertwining Network Structured TiO₂ Nanocomposite: A Promising Material for the Effective Monitoring of Dopamine and Anodic Performance in Lithium-Ion Battery. *Synth. Met.* 265, 116403. doi:10.1016/j.synthmet.2020.116403
- Viana, M. M., Soares, V. F., and Mohallem, N. D. S. (2010). Synthesis and Characterization of TiO₂ Nanoparticles. *Ceram. Int.* 36, 2047–2053. doi:10.1016/j.ceramint.2010.04.006
- Viter, R., Smyntyna, V., Starodub, N., Tereshchenko, A., Kusevitch, A., Doychoa, I., et al. (2012). Novel Immune TiO₂ Photoluminescence Biosensors for Leucosis Detection. *Proced. Eng.* 47, 338–341. doi:10.1016/j.proeng.2012.09.152
- Viter, R., Tereshchenko, A., Smyntyna, V., Ogorodnichuk, J., Starodub, N., Yakimova, R., et al. (2017). Toward Development of Optical Biosensors Based on Photoluminescence of TiO₂ nanoparticles for the Detection of Salmonella. *Sensors Actuators, B Chem.* 252, 95–102. doi:10.1016/j.snb.2017.05.139
- Wan, X. M., Zheng, F., Zhang, L., Miao, Y. Y., Man, N., and Wen, L. P. (2011). Autophagy-mediated Chemosensitization by Cysteamine in Cancer Cells. *Int. J. Cancer* 129, 1087–1095. doi:10.1002/ijc.25771
- Wang, S.-M., Dong, W.-W., Tao, R.-H., Deng, Z.-H., Shao, J.-Z., Hu, L.-H., et al. (2013). Optimization of Single-crystal Rutile TiO₂ Nanorod Arrays Based Dye-Sensitized Solar Cells and Their Electron Transport Properties. *J. Power Sourc.* 235, 193–201. doi:10.1016/j.jpowsour.2013.01.106
- Wu, Y., Wang, C.-W., Wang, D., and Wei, N. (2021). A Whole-Cell Biosensor for Point-of-Care Detection of Waterborne Bacterial Pathogens. *ACS Synth. Biol.* 10, 333–344. doi:10.1021/acssynbio.0c00491
- Yang, X., Sun, J., Cui, F., Ji, J., Wang, L., Zhang, Y., et al. (2020). An Eco-Friendly Sensor Based on CQD@MIPs for Detection of N-Acylated Homoserine Lactones and its 3D Printing Applications. *Talanta* 219, 121343. doi:10.1016/j.talanta.2020.121343
- Yaxley, J. (2016). Alkalinisation of Urine in Patients with Infections of the Urinary Tract. *Br. J. Med. Med. Res.* 13, 1–4. doi:10.9734/BJMMR/2016/23479
- Zhang, H., Wang, X., Li, N., Xia, J., Meng, Q., Ding, J., et al. (2018). Synthesis and Characterization of TiO₂/graphene Oxide Nanocomposites for Photoreduction of Heavy Metal Ions in Reverse Osmosis Concentrate. *RSC Adv.* 8, 34241–34251. doi:10.1039/C8RA06681G
- Zhu, L., Lu, Q., Lv, L., Wang, Y., Hu, Y., Deng, Z., et al. (2017). Ligand-free Rutile and Anatase TiO₂ Nanocrystals as Electron Extraction Layers for High Performance Inverted Polymer Solar Cells. *RSC Adv.* 7, 20084–20092. doi:10.1039/C7RA00134G

Conflict of Interest: The authors declare that the research was conducted in the absence of any commercial or financial relationships that could be construed as a potential conflict of interest.

Publisher's Note: All claims expressed in this article are solely those of the authors and do not necessarily represent those of their affiliated organizations, or those of the publisher, the editors, and the reviewers. Any product that may be evaluated in this article, or claim that may be made by its manufacturer, is not guaranteed or endorsed by the publisher.

Copyright © 2021 Vasudevan, Srinivasan, Neelakantan, Rayappan and Solomon. This is an open-access article distributed under the terms of the Creative Commons Attribution License (CC BY). The use, distribution or reproduction in other forums is permitted, provided the original author(s) and the copyright owner(s) are credited and that the original publication in this journal is cited, in accordance with accepted academic practice. No use, distribution or reproduction is permitted which does not comply with these terms.